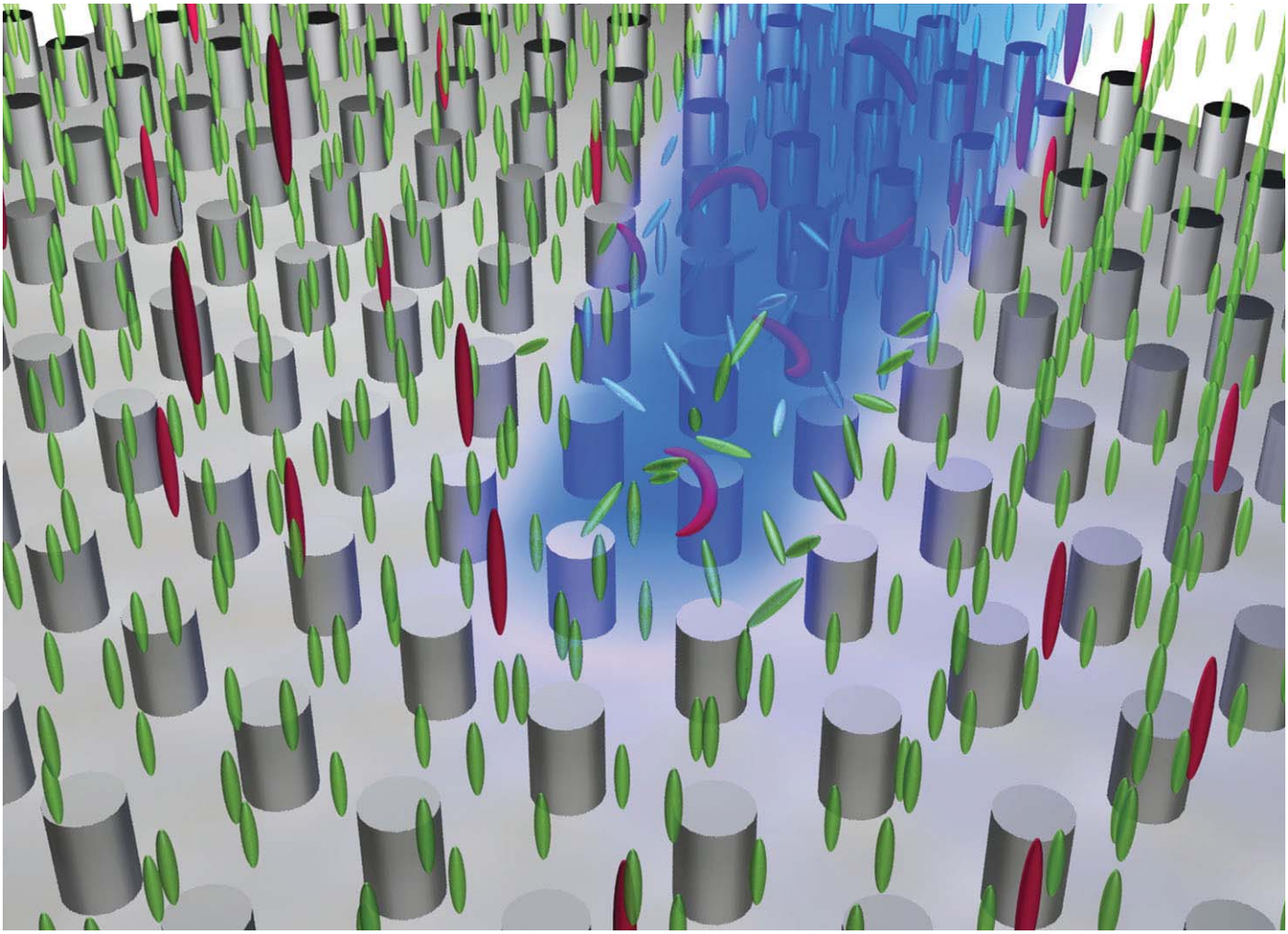

Showcasing research led by Dr Yan Jun Liu at the Institute of Materials Research and Engineering, Agency for Science, Technology and Research (A*STAR), Singapore.

Title: All-optical, polarization-insensitive light tuning properties in silver nanorod arrays covered with photoresponsive liquid crystals

A hybrid system that integrates a silver nanorod array with photoresponsive liquid crystals is demonstrated. The silver nanorod array enables homeotropic alignment of the liquid crystal molecules, which makes the optical tuning polarization-insensitive under the UV light pump.

As featured in:

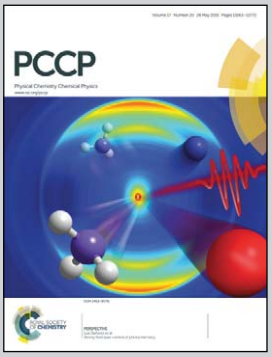

See Haitao Dai, Yan Jun Liu *et al.*, *Phys. Chem. Chem. Phys.*, 2015, **17**, 13223.

ROYAL SOCIETY OF CHEMISTRY

www.rsc.org/pccp

Registered charity number: 207890

PCCP

PAPER

Cite this: *Phys. Chem. Chem. Phys.*, 2015, **17**, 13223

All-optical, polarization-insensitive light tuning properties in silver nanorod arrays covered with photoresponsive liquid crystals

Guangyuan Si,[a] Eunice S. P. Leong,[b] Xiaoxiao Jiang,[a] Jiangtao Lv,[a] Jiao Lin,[c] Haitao Dai*[d] and Yan Jun Liu*[b]

Received 13th January 2015,
Accepted 17th February 2015

DOI: 10.1039/c5cp00185d

www.rsc.org/pccp

Active plasmonics has been an interesting and important topic recently. Here we demonstrate the all-optical, polarization-insensitive tunable manipulation of a hybrid system that integrates a silver nanorod array with photoresponsive liquid crystals. The large-area plasmonic nanorod arrays are fabricated by laser interference lithography and ion milling. By covering a layer of photoresponsive liquid crystals, tunable control of plasmon resonance is achieved under an external light pump. The silver nanorod array also enables the homeotropic alignment of the liquid crystals, which makes the all-optical tuning behavior polarization-insensitive. With its advantages of cost-effective fabrication, easy integration, all-optical control, and polarization-insensitivity, the hybrid system could be valuable in many nanophotonic applications.

Introduction

Plasmonics has been attracting extensive attention across various fields over the past two decades. The core of this field lies in the manipulation of light–matter interactions at the nanoscale with the excitation of surface plasmon resonance, which are the collective oscillations of free electrons confined at metal/dielectric interfaces. Thus far, many exciting plasmonic applications, such as super-resolution imaging,[1,2] optical cloaking,[3,4] and energy harvesting,[5–7] have been reported. However, one major drawback of the abovementioned plasmonic devices is that they serve as passive devices providing consistent outputs given the same inputs, which greatly limits their applications that may only need a little change in the sample design. Therefore, it is highly beneficial to have reconfigurable or tunable functions after the devices are fabricated, with the help of active media.

Since plasmon resonances are very sensitive to the surrounding environment of plasmonic nanostructures, varying the surrounding's dielectric properties becomes a straightforward and effective way to have active control of the surface plasmon resonance. For this purpose, liquid crystals (LCs) stand out as an excellent candidates of active media since they possess dynamic, continuous, and most importantly, reversible tuning behavior using various driving strategies.[8–14] Since LC molecules are very small, they can be conveniently integrated with nanoscale plasmonic nanostructures, and hence they are potentially useful for many active plasmonic devices.[15–23] These active plasmonic devices are of paramount importance for the future development of nanophotonic chips/circuits.[24,25] When integrating LCs with plasmonic nanostructures, the proper alignment of LCs still remains a challenge since the addition of a conventional alignment layer might affect the efficient coupling of LCs and surface plasmons. As is well known, surface grooves with suitable pitch and depth are effective in aligning LCs.[26–29] It is therefore highly possible to have controllable LC alignment using plasmonic nanostructures. In this paper, we fabricate a large-area and dense silver nanorod array using laser interference lithography and ion milling. Due to the sufficient aspect ratio of the nanorods, the silver nanorod array enables a homeotropic alignment of the LCs. By rendering the LCs photoresponsive, we demonstrate a hybrid system with all-optical, polarization-insensitive tunable properties under an external UV light pump. Our approach may open up new avenues for LC alignment using plasmonic nanostructures. The hybrid system may also find many nanophotonic applications that require polarization-insensitive operation.

Device fabrication and characterization

In our experiments, quartz substrates were first cleaned and loaded in the chamber of an electron-beam evaporator

[a] *College of Information Science and Engineering, Northeastern University, Shenyang 110004, China*
[b] *Institute of Materials Research and Engineering, Agency for Science, Technology and Research (A*STAR), 3 Research Link, Singapore 117602, Singapore. E-mail: liuy@imre.a-star.edu.sg*
[c] *School of Physics, The University of Melbourne, Vic 3010, Australia*
[d] *Tianjin Key Laboratory of Low Dimensional Materials Physics and Preparing Technology, School of Science, Tianjin University, Tianjin 300072, China. E-mail: htdai@tju.edu.cn*

(Edwards Auto 306). Subsequently, a 5 nm titanium adhesion layer and 175 nm thick Ag film were deposited at a basic pressure of 5×10^{-7} mbar. Positive resist S1805 was spin-coated onto the sample surface and baked at 180 °C on a hotplate for 2 minutes. Laser interference lithography was carried out to achieve the resist pattern, which was further used as an ion milling mask. The sample was milled using ion milling equipment (Intlvac Nanoquest ion beam etching system). During ion milling, an argon source was impinged upon the sample surface at a 10° angle, ensuring uniform removal of waste material and straight sidewalls in all features with almost negligible undercutting. The beam voltage was 300 V with a 45 V accelerating voltage and 110 mA beam current. Finally, the resist residue was removed by a Micro-posit Remover 1165. Once the Ag nanorod array was ready, we sandwiched a photoresponsive LC layer in between a quartz substrate with the nanorod array and a bare glass substrate. The thickness was controlled at ~7 μm using polystyrene microbeads. The photoresponsive LC material used in our experiments consisted of 85 wt% nematic LC, E7 (Merck), and 15 wt% photochromic LC, 4-butyl-4-methyloxyazobenzene (BMAB). Angle-resolved spectroscopic measurements for the hybrid system were performed using a UVISEL (HORIBA Jobin Yvon). All the photoresponsive spectra of the sample were taken under a continuous UV pump of ~30 seconds.

Results and discussion

Fig. 1 is the typical scanning electron microscopy (SEM) image of the Ag nanorod arrays on a quartz substrate. The measured periodicity of the two-dimensional nanorod array is ~600 nm and the whole working area is 1.5×1.5 cm^2. Based on the thickness of the silver film, the estimated aspect ratio (height to diameter) of the nanorod is ~0.6. The insets are the images of the sample before and after infiltration of the photoresponsive LCs.

Fig. 2 shows the plots of the transmission of the Ag rod arrays (600 nm period and 175 nm height) before and after LC infiltration at normal incidence. For the bare sample, one can clearly observe two resonance dips (at 635 and 756 nm, respectively) that are from the interplay between the excitation of the plasmons localized on the nanorods and diffraction resulting from the scattering by the periodic arrangement of these nanorods.[30] As a reference, the transmission spectrum of BMAB-doped LC itself with the same thickness is also shown in Fig. 2. After LC infiltration, the peak at 325 nm disappears because of the strong absorption of the BMAB molecules, while both resonance dips red-shift from 635 and 756 nm to 654 and 826 nm, respectively, because of the increased refractive index of the surroundings. One interesting point is that after LC infiltration, the hybrid system demonstrates a broadband top-flat transmission range, which is the typical feature of a bandpass filter and hence is useful for filtering applications. Under the UV light pump, the transmission of the broadband pass range is further enhanced and broadened. In addition, the resonance dips also red-shift further to 659 and 855 nm. The further transmission enhancement and dip in red-shift indicate that the effective refractive index of the surroundings (*i.e.*, the LCs) of the Ag nanorod array increases under the UV light pump since the localized surface plasmon resonance position shifts linearly with the refractive index change of the surrounding medium.[31]

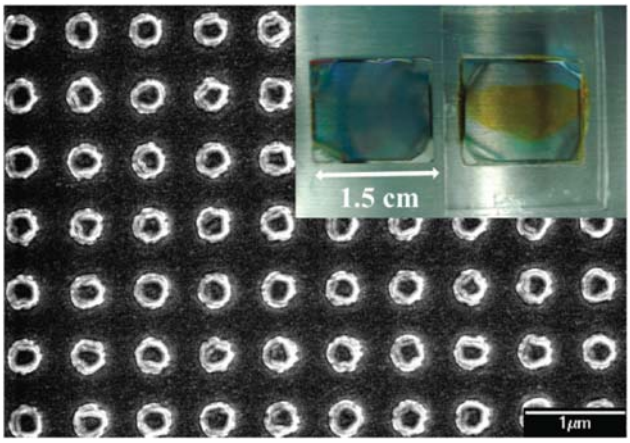

Fig. 1 Typical SEM image showing the top-view of a fabricated silver nanorod arrays. Insets are the images of the real sample before (left) and after LC (right) infiltration.

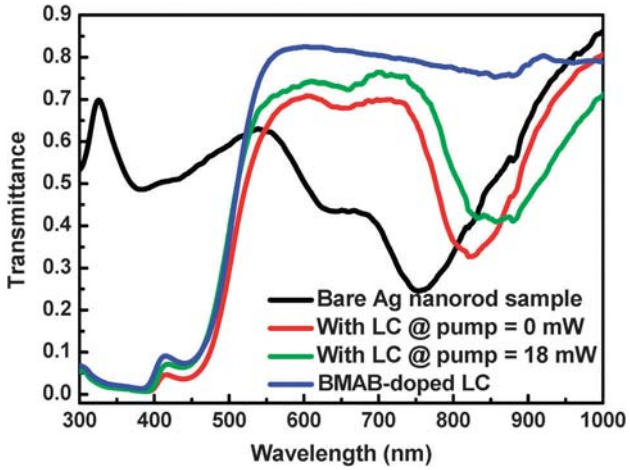

Fig. 2 Measured transmittance of the bare sample before and after LC infiltration with a UV light pump.

The all-optically tunable behavior observed in our experiments could be attributed to the *trans–cis* isomerization-induced nematic–isotropic phase change of the LCs. When the BMAB molecules absorb UV light, the *trans*-isomer transforms into the *cis*-isomer. Fig. 3 shows the measured absorption spectra of BMAB before and after the UV pump. We can clearly see that the *trans*-isomer has a main absorption peak at ~350 nm in the UV band, while the *cis*-isomer has an absorption peak at ~450 nm in the blue band. The *cis*-isomer affects the host nematic as an impurity, which disrupts the local order and forms an isotropic phase. This order change generates a photoinduced refractive index modulation. As a result, we have observed tuning behavior. It is very interesting to note that transmission is increased under the UV light pump, which is different from the

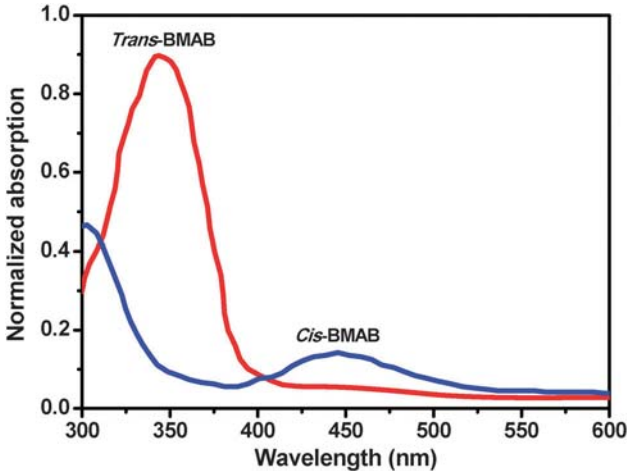

Fig. 3 The *trans–cis* isomerization of BMAB under a UV pump.

previous report with pre-set LC alignment.[18] In our previous report, we observed that when a pumping light was on, the transmission decreased owing to the decrease of the effective refractive index of the LCs seen by the probe light. We believe that this discrepancy was because of the difference of the LC alignment. In this work, although there is no surface treatment to pre-define the LC alignment, the Ag nanorod array could induce preferred alignment of the rod-like LC molecules considering their relatively high aspect ratio of ~0.6. In addition to the increase of the transmission, we also observed the redshift of the resonance dips. This redshift clearly confirms that the effective refractive index of the LCs was increased under the UV light pump. Such an index increase can only happen provided that the LC molecules form a homeotropic alignment (*i.e.*, parallel to the nanorod wall) before UV irradiation, as shown in Fig. 4(a). At the homeotropic alignment state, the probe light, regardless of its polarizations, will only experience the ordinary refractive index (n_o = 1.52) of the LCs in the LC region. As a result, the hybrid system demonstrates polarization-insensitive optical transmission. Under the UV light pump, the *trans–cis* isomerization of BMAB molecules will cause the LCs to change from the nematic phase to the isotropic phase, as shown in Fig. 4(b). In the isotropic state, the hybrid system will be again polarization-insensitive, and the empirical effective index for an isotropic LC can be estimated as $n_{iso} \cong (2n_o + n_e)/3$. For the LC, E7, used in our experiment, this value is $n_{iso} \cong 1.60$. Therefore, the probe light will experience a refractive index increase of about 0.08 under the UV light pump. This index increase is the root reason for the transmission increase and redshift. As is well known, the resonant wavelength shifts linearly with change in the refractive index, which corresponds to a refractive index sensitivity of ~360 nm per RIU (refractive index unit). Such sensitivity is comparable to other reported plasmonic sensors,[32,33] indicating that such a silver nanorod array is also potentially useful for biosensing applications. To further confirm our speculation on the LC alignment, the sample was observed between two crossed polarizers under a polarized optical microscope. Fig. 4(c) and (d) show the optical images before and after the UV light pump. We can see that both images are dark since light transmission is prohibited in both cases.

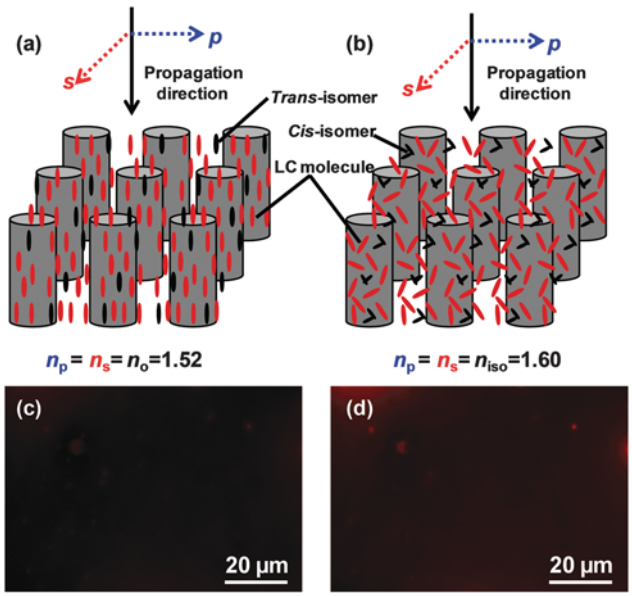

Fig. 4 The proposed model for the alignment of LC molecules inside the Ag nanorod array before (a) and after (b) the UV light pump. The observed optical images before (c) and after (d) the UV light pump between two crossed polarizers under the polarized optical microscope.

Before the UV light pump, darkness can only happen when the LC molecules align perpendicular to the substrate. However, after the UV light pump, the LC molecules demonstrate an isotropic state, which again prohibits the light transmission between two crossed polarizers. Both observed dark states indicate that the optical tuning is polarization-insensitive. However, we noticed that the observed optical image after the UV light pump became slightly brighter than that before the light pump, which could be mainly attributed to more scattering; moreover, this is caused by the *cis*-isomer-induced disruption of the local nematic order of the LCs. From the above discussion, a distinct advantage of our hybrid system is its polarization-independent optical behaviour in transmission at normal incidence, which is important for many optical devices that require polarization-insensitive operation.

We further investigated the incident-angle-dependent transmission properties of the hybrid system. Fig. 5 shows the effect of the pumping power on the transmission at a fixed incident angle of 20°. From Fig. 5(a), one can see that the broadband transmission wavelength range shows non-flattened features. This could be mainly attributed to nonsymmetrical plasmon excitation and nonlinear wavelength-dependent transmission enhancement. As the pump power increases, the transmission intensity also increases and then saturates at a certain value. After that, the transmission intensity decreases. The transmission drop could result from the decrease of the effective refractive index of the LCs, which is possibly attributed to the thermally induced nematic–isotropic phase transition of the LCs and is caused by the absorption-induced temperature increase.[34] In addition, another transmission peak between 350 nm and

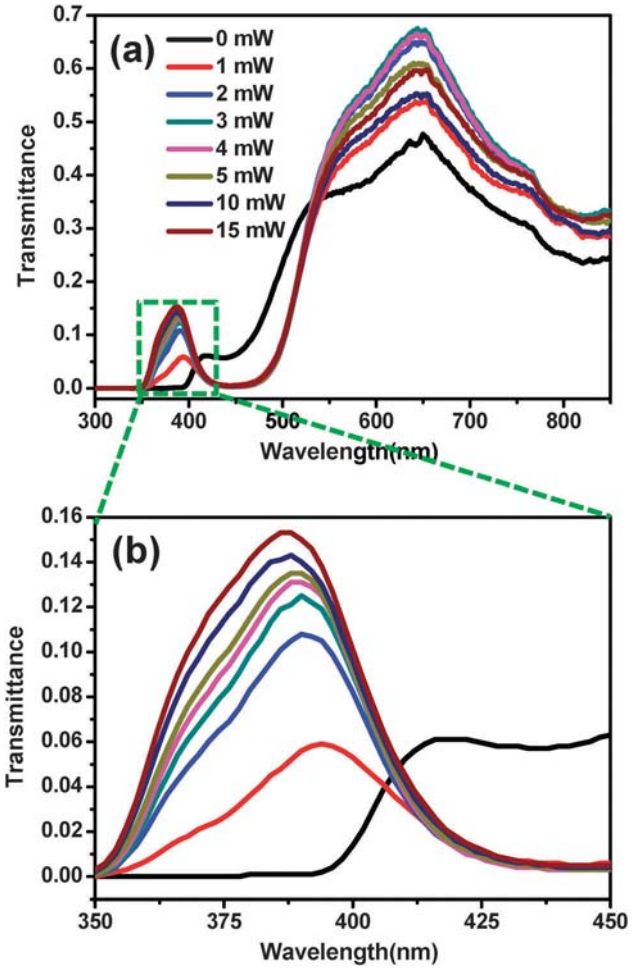

Fig. 5 (a) Effect of the pumping power on the transmission at a fixed incident angle of 20° and (b) magnified view of (a) in the wavelength range of 350–450 nm.

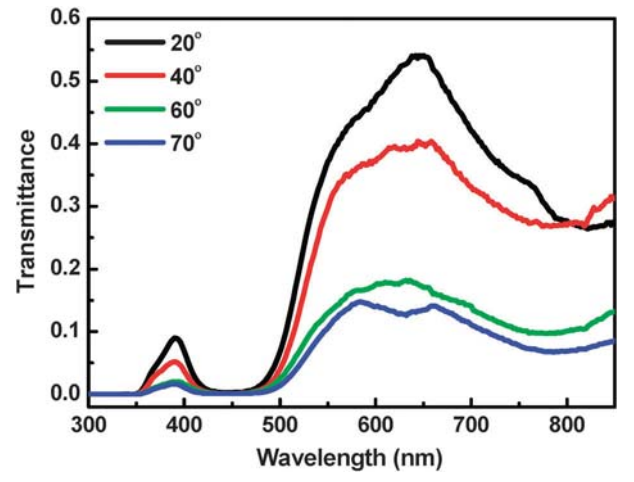

Fig. 6 Measured incident-angle-dependent transmittance at the fixed pumping power of 15 mW.

400 nm appears with increase in the pumping power, which can be observed more clearly in the magnified spectra in Fig. 5(b). This is the typical *trans–cis* isomerization signature of the BMAB molecules, which is slightly tailored by the original transmission peak at 325 nm of the bare nanorod array (see Fig. 2). Fig. 6 shows the effect of the incident angle at a fixed pumping power of 15 mW. As the incident angle increases, the transmission drops greatly. At this pumping power, the photoresponsive LCs demonstrate the isotropic state. Therefore, the transmission change depends largely on the excitation of the nanorod plasmons.

Conclusions

In summary, we have demonstrated an all-optical, polarization-insensitive light tuning based on a hybrid system that integrates a silver nanorod array with photoresponsive liquid crystals. The large-area and dense plasmonic nanorod array with sufficient heights enables the homeotropic alignment of the LCs, which makes the optical tuning of the hybrid system polarization-insensitive at normal incidence. With its advantages in cost-effective fabrication, easy integration, all-optical control, and polarization-insensitivity, the hybrid system could be potentially useful for many nanophotonic applications.

Acknowledgements

E. S. P. Leong and Y. J. Liu acknowledge financial support from the Agency for Science, Technology and Research (A*STAR) under the grant No. 12302FG012, 0921540098, and 0921540099. This work was partially supported by the National Natural Science Foundation of China (grant No. 61405031). H. T. Dai also acknowledges the funding support from the National Natural Science Foundation of China under grant No. 61177061.

Notes and references

1 J. B. Pendry, *Phys. Rev. Lett.*, 2000, **85**, 3966–3969.
2 N. Fang, H. Lee, C. Sun and X. Zhang, *Science*, 2005, **308**, 534–537.
3 J. B. Pendry, D. Schurig and D. R. Smith, *Science*, 2006, **312**, 1780–1782.
4 I. I. Smolyaninov, V. N. Smolyaninova, A. V. Kildishev and V. M. Shalaev, *Phys. Rev. Lett.*, 2009, **102**, 213901.
5 H. A. Atwater and A. Polman, *Nat. Mater.*, 2010, **9**, 205–213.
6 A. Aubry, D. Y. Lei, A. I. Fernandez-Dominguez, Y. Sonnefraud, S. A. Maier and J. B. Pendry, *Nano Lett.*, 2010, **10**, 2574–2579.
7 O. Andreussi, A. Biancardi, S. Corni and B. Mennucci, *Nano Lett.*, 2013, **13**, 4475–4484.
8 Y. J. Liu and X. W. Sun, *Appl. Phys. Lett.*, 2007, **90**, 191118.
9 C.-R. Lee, J.-D. Lin, B.-Y. Huang, S.-H. Lin, T.-S. Mo, S.-Y. Huang, C.-T. Kuo and H.-C. Yeh, *Opt. Express*, 2011, **19**, 2391–2400.
10 V. A. Greanya, A. P. Malanoski, B. T. Weslowski, M. S. Spector and J. V. Selinger, *Liq. Cryst.*, 2005, **32**, 933–941.
11 Y. J. Liu, X. Y. Ding, S.-C. S. Lin, J. J. Shi, I.-K. Chiang and T. J. Huang, *Adv. Mater.*, 2011, **23**, 1656–1659.

12 V. K. S. Hsiao and C.-Y. Ko, *Opt. Express*, 2008, **16**, 12670–12676.
13 Y. J. Liu, Y. B. Zheng, J. Shi, H. Huang, T. R. Walker and T. J. Huang, *Opt. Lett.*, 2009, **34**, 2351–2353.
14 Y. J. Liu, Z. Y. Cai, E. S. P. Leong, X. S. Zhao and J. H. Teng, *J. Mater. Chem.*, 2012, **22**, 7609–7613.
15 P. A. Kossyrev, A. Yin, S. G. Cloutier, D. A. Cardimona, D. Huang, P. M. Alsing and J. M. Xu, *Nano Lett.*, 2005, **5**, 1978–1981.
16 Y. J. Liu, Q. Hao, J. S. T. Smalley, J. Liou, I. C. Khoo and T. J. Huang, *Appl. Phys. Lett.*, 2010, **97**, 091101.
17 Y. J. Liu, Y. B. Zheng, J. Liou, I. K. Chiang, I. C. Khoo and T. J. Huang, *J. Phys. Chem. C*, 2011, **115**, 7717–7722.
18 Y. J. Liu, G. Y. Si, E. S. P. Leong, N. Xiang, A. J. Danner and J. H. Teng, *Adv. Mater.*, 2012, **24**, OP131–OP135.
19 W. Chang, J. B. Lassiter, P. Swanglap, H. Sobhani, S. Khatua, P. Nordlander, N. J. Halas and S. Link, *Nano Lett.*, 2012, **12**, 4977–4982.
20 A. E. Cetin, A. Mertiri, M. Huang, S. Erramilli and H. Altug, *Adv. Opt. Mater.*, 2013, **1**, 915–920.
21 L. De Sio, A. Cunningham, V. Verrina, C. M. Tone, R. Caputo, T. Burgi and C. Umeton, *Nanoscale*, 2012, **4**, 7619–7623.
22 L. De Sio, T. Placido, S. Serak, R. Comparelli, M. Tamborra, N. Tabiryan, M. Lucia Curri, R. Bartolino, C. Umeton and T. Bunning, *Adv. Opt. Mater.*, 2013, **1**, 899–904.
23 G. Si, Y. Zhao, E. S. P. Leong and Y. J. Liu, *Materials*, 2014, **7**, 1296–1317.
24 E. Ozbay, *Science*, 2006, **311**, 189–193.
25 R. Zia, J. A. Schuller, A. Chandran and M. L. Brongersma, *Mater. Today*, 2006, **9**, 20–27.
26 D. W. Berreman, *Phys. Rev. Lett.*, 1972, **28**, 1683–1686.
27 D. W. Berreman, *Mol. Cryst. Liq. Cryst.*, 1973, **23**, 215–231.
28 H. Takahashi, T. Sakamoto and H. Okada, *J. Appl. Phys.*, 2010, **108**, 113529.
29 Y. J. Liu, W. W. Loh, E. S. P. Leong, T. S. Kustandi, X. W. Sun and J. H. Teng, *Nanotechnology*, 2012, **23**, 465302.
30 B. Auguié and W. L. Barnes, *Phys. Rev. Lett.*, 2008, **101**, 143902.
31 Y. B. Zheng, B. K. Juluri, X. Mao, T. R. Walker and T. J. Huang, *J. Appl. Phys.*, 2008, **103**, 014308.
32 A. De Leebeeck, L. K. Swaroop Kumar, V. de Lange, D. Sinton, R. Gordon and A. G. Brolo, *Anal. Chem.*, 2007, **79**, 4094–4100.
33 E. S. P. Leong, Y. J. Liu, J. Deng, Y. T. Fong, N. Zhang, S. J. Wu and J. H. Teng, *Nanoscale*, 2014, **6**, 11106–11111.
34 J. Li, S. Gauza and S. Wu, *J. Appl. Phys.*, 2004, **96**, 19–24.